Ain Shams Engineering Journal 14 (2023) 102010

Contents lists available at ScienceDirect

Ain Shams Engineering Journal

journal homepage: www.sciencedirect.com

Thermal and vibratory response of sprung square cylinder with four nature-inspired fin-shaped bumps

Amir Hossein Rabiee [a], Somayeh Davoodabadi Farahani [a,*], Amir Mosavi [b,c,*]

[a] School of Mechanical Engineering, Arak University of Technology, 38181-41167 Arak, Iran
[b] Faculty or Engineering, Obuda University, Budapest, Hungary
[c] Institute of Information Society, University of Public Service, Budapest, Hungary

ARTICLE INFO

Article history:
Received 29 March 2022
Revised 15 July 2022
Accepted 6 October 2022
Available online 20 October 2022

Keywords:
Heat transfer
Elastically-mounted cylinder
Fin-shaped bumps
Flow-induced vibration

ABSTRACT

Nature provides man with various interesting structures, offering him a constant source of manufacturing tools and invention. The main purpose of the present paper is to investigate the effect of shark-inspired fins, which are installed on the top and bottom plates of a sprung cylinder on the vibration response and heat transfer of square cylinder. Two fin sizes, i.e. small and big, are used. Three configurations for the fins on the top and bottom plates of the square cylinder are considered: at the corners of the square cylinder, spaced from the corners, and in the middle of the plates. The results indicate that adding fins increases the amplitude of vortex-induced vibrations and extends the lock-in region which is both intensified as the size of fins increases. In particular, for the cylinder equipped with small fins in configurations 1–3, the maximum VIV amplitude increases by, respectively, 36 %, 57 % and 52 % compared with the plain cylinder. In contrast, shark fins can lower the galloping amplitude by as much as 87 % and shrink the galloping zone such that for big fin size in the second and third configurations, the galloping zone and its corresponding vortex-shedding mode are not observed. Adding fins to the cylinder augments heat transfer. The increase in mean Nusselt number depends on vortex-shedding mode, and the rise in Nusselt number is higher in the 2P + 2S mode.

1. Introduction

Flow-induced vibration (FIV) occurs when a structure is excited to vibrate due to the destabilizing forces exerted from the fluid flow. If the structure is completely rigid and restrained, the vortex generation frequency can be estimated as a function of the non-dimensional Strouhal number. Experiments show that on a comparatively extensive range of Reynolds numbers, the Strouhal number is almost constant and close to 0.2 [1,2]. By contrast, when a structure can oscillate, i.e. a flexible structure with non-rigid supports, a phenomenon called lock-in is observed over a range of certain parameters. At low flow velocities, the vortex-shedding frequency is analogous to that for a rigid fixed structure and is controlled by the non-dimensional Strouhal number [3,4]. When the flow velocity rises, the vortex generation frequency approaches the oscillation frequency of oscillator and is no longer governed by the Strouhal number. In fact, the vortex generation frequency synchronizes itself with the oscillation frequency of structure and locks on it. As the former frequency comes close the natural frequency of oscillator, resonance happens and the cylinder oscillations, so called the vortex-induced vibrations (VIV), tend to rise [5,6]. Such vibrations can cause damage and irreparable destruction to the structure. Reduced service life and even degradation due to FIV impose high costs to different industries. This is especially important in the case of heat exchangers, chimneys, nuclear exchangers, bridge foundations, piers and coastal equipment, oil platforms, drilling rigs and cooling towers [7,8]. Since the reduction of oscillating forces and impeding the vortex-shedding increase the useful life and stability of structures, this issue is considered to be a practical engineering problem. In recent years, extensive investigations have been focused on reducing the vortex-shedding and consequently FIV using various passive and active methods [9–11]. Passive control methods are simpler to

* Corresponding author.
E-mail addresses: sdfarahani@arakut.ac.ir (S.D. Farahani), amir.mosavi@kvk.uni-obuda.hu (A. Mosavi).

Peer review under responsibility of Ain Shams University.

Production and hosting by Elsevier

https://doi.org/10.1016/j.asej.2022.102010
2090-4479/

Nomenclature

U	Velocity(m/s)
h_{mean}	Mean value of total heat transfer coefficient (W/m^{2}K)
$h_{ave.}$	Spatial average of the convective heat transfer coefficient (W/m^{2}K)
C_L	Lift coefficient
C_P	Heat capacity (J/kgK)
F_L	Lift force (N)
L_d	Downstream length (m)
L_u	Upper length (m)
T_∞	Temperature of inlet fluid (K)
T_s	Surface temperature (K)
U_∞	Inlet velocity (m/s)
U_s	Square velocity (m/s)
f_n^*	Reduced natural frequency
m^*	Non-dimensional mass of the cylinder
$\dot{y}$	Velocity of the square cylinder (m/s)
$\ddot{y}$	Acceleration of the square cylinder (m/s^2)
A	Area (m^2)
D	Cylinder diameter (m)
h	Convection heat transfer coefficient (W/m^{2}K)
H	Rectangular computational domain of the height (m)
k	Thermal conductivity coefficient (W/mK)
$\text{Nu}_{\text{ave.}}$	Spatial average of the Nusselt number
Nu_{mean}	Mean value of the overall Nusselt number
Nu	Nusselt number
P	Pressure (Pa)
Re	Reynolds number
t	Time (s)
T	Temperature (K)
x, y	Coordinate
Y	Non-dimensional movement of the cylinder
c	Damping coefficient
ks	Spring stiffness
m	Mass(kg)
y	Displacement of the square cylinder(m)

Greek

ρ	Density(kg/m^3)
v	Kinetic viscosity(m^2/s)
ω_n	Natural frequency
ζ	Damping ratio
χ	Outward vector of the plane normal to the cylinder

implement and do not require an external energy source, and are thus widely used to mitigate structural vibrations [12]. FIV control methods such as simple and helical bump, wavy cylinders, helical strakes, wire meshes and small-size tabs can usually be adopted to alter the mechanism of vortex-shedding and consequently reduce the fluctuations brought about by altering or modifying the form and geometry of bluff-body [13].

For example, Owen, et al. [14] experimentally examined the amplitude of VIV and the drag coefficient associated with a circular cylinder incorporating hemispherical bumps. They showed that adding a bump to the cylinder could reduce the drag coefficient by 25 % and suppress the vortex-shedding. Constantinides and Oakley Jr [15] used the second-order finite element method (FEM) to study the vortex-induced motion of a circular-section cylinder. They observed that helical strakes with the geometrical characteristic $P/H = 0.25D/15.0D$ (in which H and P is the strake height and pitch) can perfectly attenuate the amplitude of oscillations in the synchronization region. Based on a sequence of empirical experiments, Zeinoddini, et al. [16] examined the FIV amplitude of rough and smooth cylinders in horizontal and vertical configurations. They found that trinary strakes by the geometric characteristics displayed a similar behavior in reducing the amplitude of VIV in both arrangements. Huera-Huarte [17] studied the effect of wire meshes of different sizes and densities on the vibration of a cylinder. By examining the vibration response and the amplitude of drag coefficient on the cylinder, they determined the condition leading to the most reduction in VIV: 95 % in the amplitude of the cylinder oscillations and 20 % in the drag coefficient. Based on a series of experimental tests, Senga and Larsen [18] evaluated the forced vibrations of straked circular cylinders with different configurations. They tried to predict the straked cylinder response using hydrodynamic coefficients and empirical models. Assi and Bearman [13] examined the VIV of a wavy cylinder from the perspective of vibration and frequency response, and then compared the results with those of a plain cylinder. They realized that the vortical structure did not differ from that of the plain cylinder. Aguirre-López, et al. [19] evaluated the flow field round a baseball modeled as a circular cylinder. Their objective was to examine the influence of a single bump placed at different angles relative to the horizontal axis on the aerodynamic coefficients. The drag coefficient and friction pressure were found to be directly proportional to the lift coefficient for a single-bump cylinder. Xu, et al. [20] practically explored the vibration response of side-by-side elastic cylinders with and without helical strakes. They displayed that for the case where one of the cylinders had a strake, the FIV amplitude decreased. For the case where both tandem cylinders equipped with helical strakes, the control method performed as satisfactorily as that seen for an isolated cylinder.

Kang, et al. [21] inspected the effects of bumps on the energy cycle and free vibrations of a cylinder in low-Reynolds flows. They also inspected the effects of the circumferential bumps on vortex-induced vibration of a cylinder at low Reynolds number of 150. They realized that the energy transfer ratio increased significantly when the bumps were placed at $\theta = 60^\circ$ or $\theta = 75^\circ$. In some of the methods mentioned above, delaying the flow separation leads to a reduction in lift and drag forces, hence decreasing the heat transfer. In certain studies, in addition to studying VIV, heat transfer has also been investigated. Kang, et al. [21] investigated the heat transfer of a cylinder equipped with splitter plates in the cross flow, and observed that lowering the size of vortices and narrowing them reduced the amount of heat transfer.

Aside from VIV, galloping is another subset of FIV specific to cylinders with non-circular cross-sections as in a square-section cylinder. Galloping is a self-excitation instability that leads to low-frequency/high-amplitude vibrations in the range of Reynolds numbers higher than those of VIV [5,22]. In the galloping region, the cross-flow motions of the body create destabilizing forces, which further growth these motions. Once the inlet velocity exceeds the galloping critical value, the magnitude of oscillations rises continuously as the flow velocity increases. One of the non-circular bluff bodies considered as a fundamental case in vibration analysis is the square cylinder. As discussed earlier, several methods have been used to reduce the VIV in circular cylinders, while few researches have been conducted on square cylinders. For example, Wu, et al. [23] used numerical simulations to examine the vortex-induced vibration of a twisted square cylinder with several twist angles along the lines of 0° and 45°. They showed that the twisted faces of this square cylinder change the flow separation

points along with the vortex-shedding frequency, which affects the distribution of aerodynamic forces exerted to the square cylinder. Dash, et al. [24] numerically inspected the efficacy of double splitter plates in drag reduction of square-section cylinders and the resulting improvement in the wake regime. Using two splitter plates with optimized length and distance, they could annihilate the vortical structure and greatly decrease the lift and drag coefficients on the square cylinder.

The number of geometries whose special features can be tailored to meet our demands is aplenty. For instance, fishes can actively move their fins through the water, thus adjusting the flow around them. In recent years, there have been many attempts at modifying the flow or enhancing the heat transfer in various applications using the shape of the fins and body of these creatures [25–28]. For instance, inspiring from the protrusions on shark fins, Zhu and Gao [29] could increase the FIV amplitude of a circular cylinder for energy harvesting purposes. They utilized two symmetric fin-shaped strips with different installation angles to improve the efficacy of the energy harvesting system. The effect of the presence of the cylinder on the heat transfer of nanofluid in a wave-shaped chamber has been investigated by Hatami and Safari [30]. They found that heat transfer increases when the cylinder is located in the center of the chamber. In a study, Hatami, et al. [31] investigated the movement of spherical particles in the flow using the Ms-DTM method. The use of forced vibrations of the cylinder in the presence of nanofluids [32,33] and magnetic field [34] can be effective on heat transfer in the desired geometries.

The above literature review indicates that despite the large number of studies on the effect of adding protuberances or bumps with different geometries on the vortical structure and free vibrations of circular cylinders, few studies have dealt with the impact of employing any protrusion on the heat transfer and free oscillations of cylinders with square cross-section. Also, no study has been carried out on the effect of adding a fin on the free vibrations of a square cylinder or its heat transfer. In the present article which is inspired by nature, certain fins similar to those on sharks are considered on the top and bottom faces of a square cylinder. This is followed by a comprehensive evaluation of the effect of fin size and position on the vortex shedding mechanism, lift and drag forces, heat transfer and VIV of the square cylinder using numerical fluid–structure simulations.

2. Numerical approach

2.1. Governing equation

Using numerical studies, the current paper investigates the influence of fins on the vibrations and heat transfer of an oscillating sprung cylinder with one degree of freedom, as demonstrated in Fig. 1a. The dimensions of this square cylinder and the solution domain are taken as $D \times D$ and $35D \times 20D$. In addition, the arrangement of the square cylinder in the solution domain is displayed in Fig. 1a. The temperature of the cylinder surface is higher than that of the surrounding fluid. As observed in Fig. 1b, the shape of the fins is inspired by shark fins. To evaluate the effect of fin size and location on the top and bottom plates of the square cylinder on the velocity and temperature fields, three different configurations, i.e. Configs. 1–3, and two different sizes, i.e. small and big, are assumed as depicted in Fig. 1b. In Config. 1, four fins are exactly installed in the corners of the square cylinder. The fins in Config. 2 are transferred a little backward. In Config. 3, the fins are next to each other in the center of top and bottom plates of the square cylinder. Fig. 2a demonstrates the actual size of small and big fins in the three mentioned configurations. For an incompressible unsteady flow with the density ρ, the kinematic viscosity ϑ, the thermal conductivity k and the heat capacity at constant pressure C_p, the equations of conservation of mass, momentum and energy are written as [1,2].

$$\vec{\nabla}.\vec{U} = 0 \tag{1}$$

$$\frac{\partial \vec{U}}{\partial t} + (\vec{U} - \vec{U}_s).\vec{\nabla}U = -\frac{1}{\rho}\vec{\nabla}P + v\nabla^2\vec{U} \tag{2}$$

$$\rho C_p(\frac{\partial T}{\partial t} + (\vec{U} - \vec{U}_s).\vec{\nabla}T) = k\nabla^2 T \tag{3}$$

where $t, T, U, U_s, P, \rho, C_p, kand\upsilon$ are time, temperature, flow velocity, dynamic mesh velocity , static pressure, fluid density, specific heat capacity, thermal conductivity coefficient and kinetic viscosity, respectively. The flow enters the left boundary of solution domain with the velocity U_∞ and temperature T_∞. The $\frac{\partial \vec{U}}{\partial y} = 0$ for velocity and constant temperature (T_∞) are assumed at the upper and lower boundaries of the solution domain. In contrast, the no-slip condition and constant temperature (T_s) are posited for the square cylinder and its fins. A detailed representation of boundary conditions is displayed in Fig. 1a. Throughout the study, the definition of Reynolds number, convective heat transfer coefficient and Nusselt number are taken as [2].

$$Re = U_\infty D/\nu \tag{4}$$

$$h = -\frac{k}{T_s - T_\infty}\frac{\partial T}{\partial \chi_{cylinder}} \tag{5}$$

$$Nu = hD/k \tag{6}$$

where χ is the outward vector of the plane normal to the cylinder. The spatial average of the convective heat transfer coefficient, $h_{ave.}(t)$, and the mean value of total heat transfer coefficient, h_{mean}, are, respectively, defined as.

$$h_{ave.}(t) = (\frac{1}{A}\iint_A hdA) \tag{7}$$

$$h_{mean} = (\frac{1}{\tau}(\int_0^\tau (\frac{1}{A}\iint_A hdA)dt)) \tag{8}$$

Also, the spatial average of the Nusselt number, $Nu_{ave.}$, and the mean value of the overall Nusselt number, Nu_{mean}, are defined as.

$$Nu_{ave.} = \frac{h_{ave.}(t)D}{k} \tag{9}$$

$$Nu_{mean} = \frac{h_{mean}D}{k} \tag{10}$$

When free flow hits the square cylinder, oscillating forces are exerted to its body as a result of vortex-shedding. Depending on the number of degrees of freedom, this phenomenon yields structural vibrations if the cylinder is either elastic or mounted on an elastic foundation. Here, the oscillation of the rigid square cylinder is perpendicular to the free flow direction, and a simple mass-spring-damper system is used to model its behavior as in [35,36].

$$\ddot{y} + 2\zeta\omega_n\dot{y} + \omega_n^2 y = F_L/m \tag{11}$$

where m, ks and c are the mass, spring stiffness and damping coefficient, respectively. Also, $\omega_n = \sqrt{ks/m}$ and $\zeta = c/2\sqrt{ksm}$ are the natural frequency and the damping ratio, respectively. Furthermore, F_L is the lift force, and $(y, \dot{y}, \ddot{y})$ are, respectively, the displacement, velocity and acceleration of the square cylinder in the cross-flow

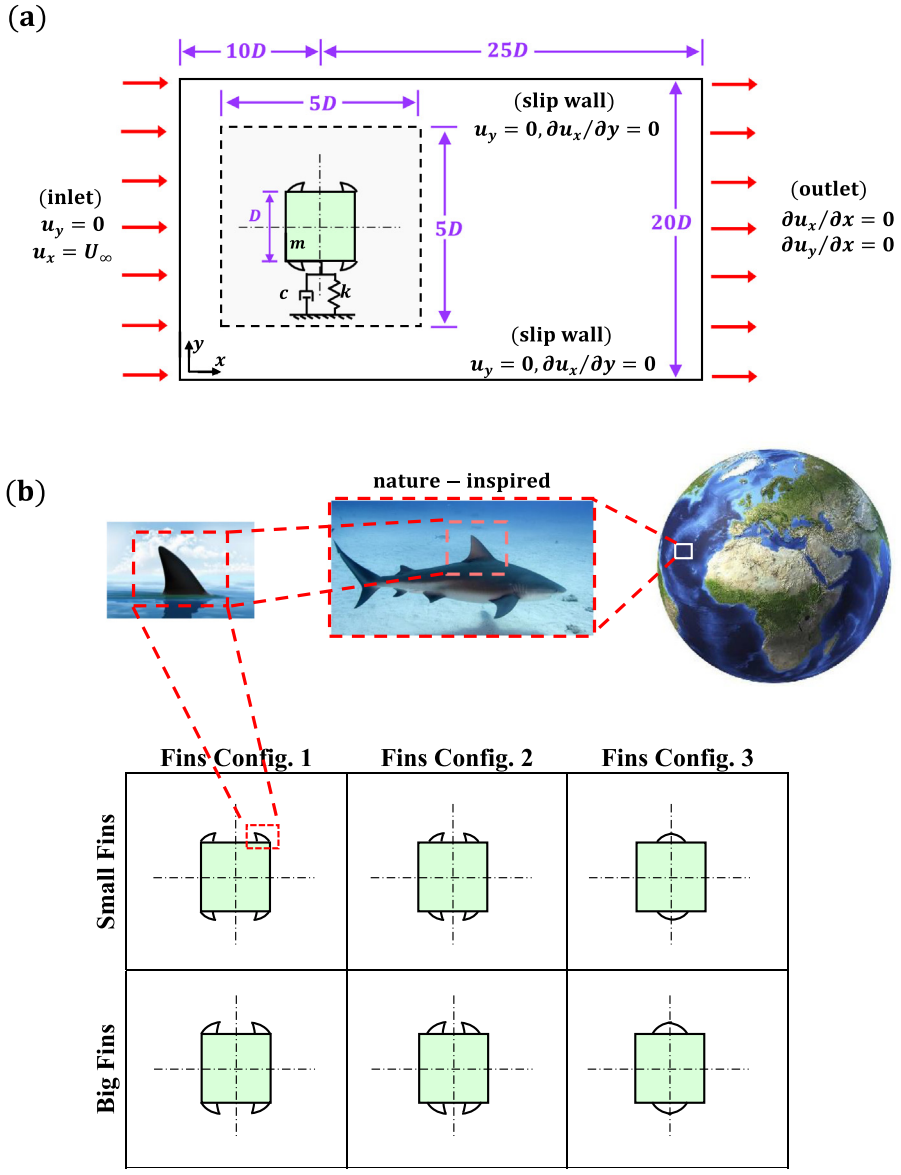

Fig. 1. a) General problem configuration and boundary conditions, and b) Different configurations of utilized fins.

direction. The non-dimensional form of Eq. (11) is derived as [35,36].

$$\ddot{Y} + 4\pi f_n^* \zeta \dot{Y} + (2\pi f_n^*)^2 Y = (2C_L/\pi m^*) \tag{12}$$

where $Y = y/D$ is the non-dimensional movement of the cylinder and $\left(Y, \ddot{Y}\right)$ are the corresponding terms of velocity and accerlation in the cross-flow direction. Also, m^* is the non-dimensional mass of the cylinder and $f_n^* = \left(\frac{D}{2\pi U_\infty}\right)\sqrt{ks/m}$ is the reduced natural frequency. The main reason for modeling the vibration behavior of a elastically-mounted cylinder in the form of a one-degree-of-freedom mass-spring-damper system is the predominance of the transverse (y-direction) displacement amplitude compared to the streamwise (x-direction) counterpart; So that the ratio of the maximum amplitude of transverse motion to the streamwise vibrations for the plain square cylinder in the lock-in and galloping regions are calculated as 100 and 12, respectively [36].

2.2. Solution procedure

The governing equations are numerically solved according to the finite volume technique using ANSYS Fluent. The second-order upwind procedure is exploited to interpolate the flux terms on the surface of elements. The second-order upwind scheme is accurate enough to predict complex phenomena in the region of flow separation and cylinder wake [11]. SIMPLE procedure is also utilized to link the pressure and velocity fields. The lift force on the cylinder for the transient solution is found using the explained method, then read by the user-defined function (UDF) code. Accordingly, the net force on the cylinder from the damper, spring, and fluid flow is obtained. Next, the acceleration and velocity for the solution time step are determined. This is followed up by updating the computational mesh based on the cylinder motion which produces a new mesh in the next iteration. An unstructured mesh with triangular elements is used in the present study. The mesh elements in the proximity of walls and behind the cylinder are selected to be very fine so that dependent variables that display a notable gradient in these regions can be estimated with reason-

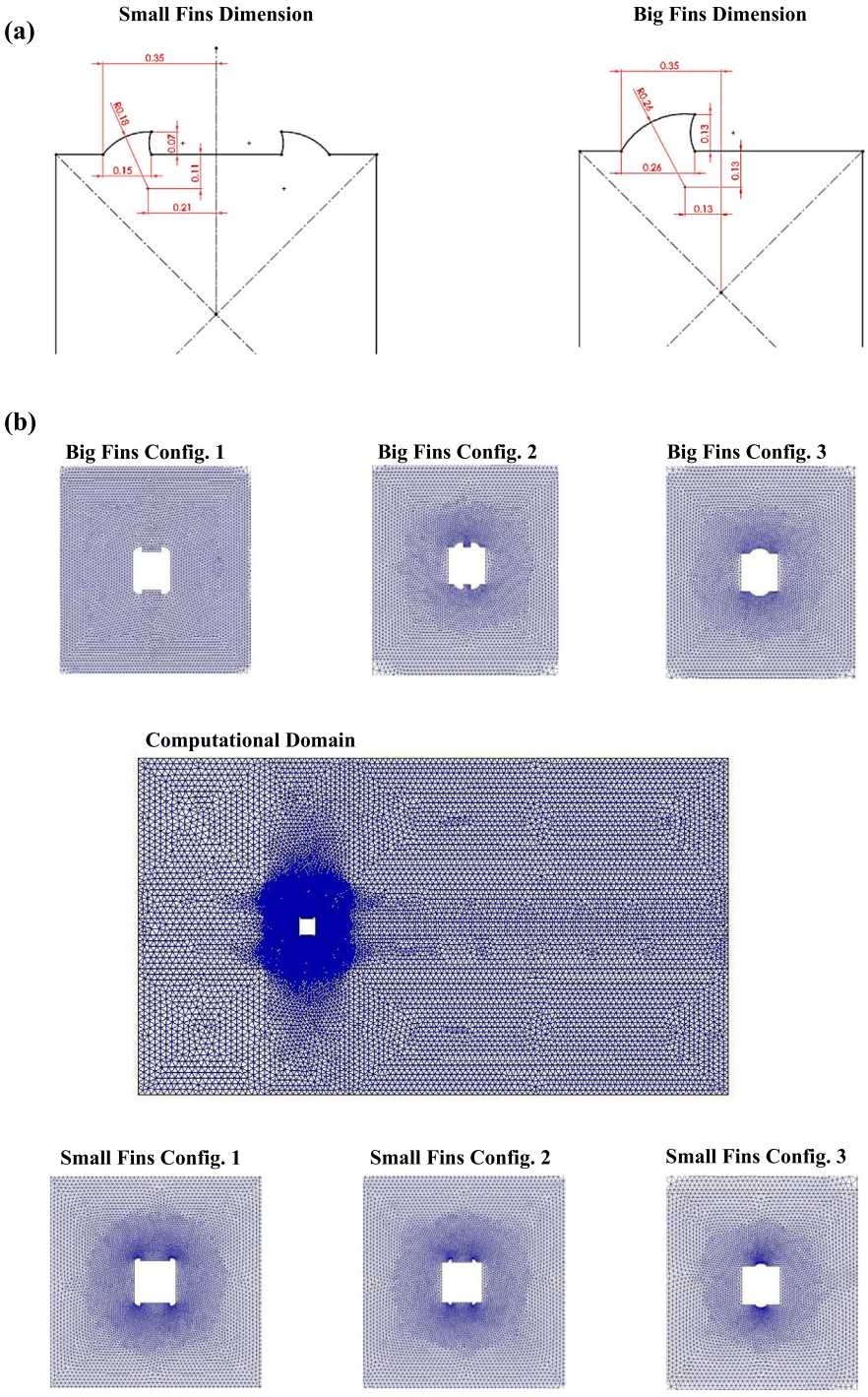

Fig. 2. a) Actual size of adopted fins, and b) Utilized computational domain.

able accuracy. Irrespective of initial conditions, the flow field in this problem attains a stable periodic state after enough time. This study assumes similar initial conditions so that step-by-step comparison of all geometric configurations is possible. To this aim, the flow field at the beginning of each numerical solution is considered to be stationary. The numerical results should be independent of the size of grid elements. Mesh independency is studied using several different grids, leading to a mesh shown in Table 1. For this purpose, three meshes with different number of nodes have been considered and the lift coefficient has been estimated for each mode. The results show that the difference for C2 mode is the lowest compared to C3. Therefore, the mesh corresponding to the C2 mode for Fin config.1 is selected to continue the solution. For Fin config. 2 and 3, this check has been done to choose the suitable mesh and shown in Fig. 2.

Table 1
The efficacy of grid size on the current solution for *Re* = 100.

Cases	C1	C2	C3
Cells number	9105	21,400	65,300
C_L^{max}	0.383	0.34	0.3381
Error (%)	13 %	0.52 %	0

The convergence criteria for the continuity equation, momentum and energy are considered to be 0.001, 0.00001 and 0.000001, respectively. This implies the selection of an optimal mesh for a desired problem. Choosing the right time step decreases the wall-clock time, thus the rise in computational speed. In the end, a time step of 0.01 s is preferred.

The readers are advised to visit [2,37] for more details on the numerical solution method and the fluid–solid interaction. In the following, to validate the utilized numerical solution, the obtained results for both thermal and vibration sections have been compared with the literature. First, the mean Nusselt number of a square cylinder with $Pr = 0.7$ in terms of Reynolds number has been compared with the results obtained in Ref. [38]. As can be seen in Fig. 3a, the results of the present work have shown a very good agreement with the results obtained from the mentioned reference; So that the error percentage for all considered Reynolds numbers is below 2 % and in most cases below 1 %. Second, in order to validate the combination of flow and structure solution, the parameters of the reduced natural frequency, non-dimensional mass of the cylinder, and the damping ratio according to the Ref. [39]; are considered as 0.1439, 10, and 0, respectively, and the maximum transverse displacement of the square cylinder in terms of Reynolds number is shown in the Fig. 3b. As can be seen, the results of the present work are in good agreement with the results obtained from the mentioned reference.

3. Numerical results

This study investigates how adding fins to a square cylinder oscillating in the cross-flow direction affects its vibrations and heat transfer characteristics. To this end, four shaped bumps inspired by shark fins are considered in three different configurations and two sizes. To examine the effect of fins in both synchronization and galloping regions, numerical simulations are performed at Reynolds numbers ($60 \leq \mathrm{Re} \leq 230$). The non-dimensional mass of the cylinder is equal to 10 and the natural frequency is defined as $f_n^* = f_n D/U_\infty = 14.39/\mathrm{Re}$. Moreover, a rectangular computational domain of the height $H = 20D$ and upstream and downstream boundaries of $(L_u, L_d) = (10D, 25D)$ is considered with 35,764 elements.

Fig. 4 displays the changes in the maximum non-dimensional cylinder displacement with Reynolds number for the small fins of Configs. 1–3. Also shown are the variations in the lift and drag coefficients on the cylinder in terms of Reynolds number. Furthermore, for all cases, the response of a plain cylinder is added for comparison. As mentioned earlier, for a plain square cylinder, when the flow velocity rises, the VIV is the first phenomenon that occurs first. This is where the vortex separation frequency comes close to the oscillator natural frequency. In the frequency synchronization (lock-in) region, self-excitation vibrations with a relatively large amplitude are detected for the square cylinder. After the cylinder exits the lock-in region, once the inlet velocity exceeds a critical value, it enters the galloping zone, which is specific to cylinders with non-circular sections. In the galloping zone, the structural movements lead to the generation of aerodynamic forces, which further increase these oscillations. One observes here that the amplitude of galloping vibrations is much greater than that of VIV (almost 5 times larger). As a result, the reduction in galloping amplitude is more important than VIV.

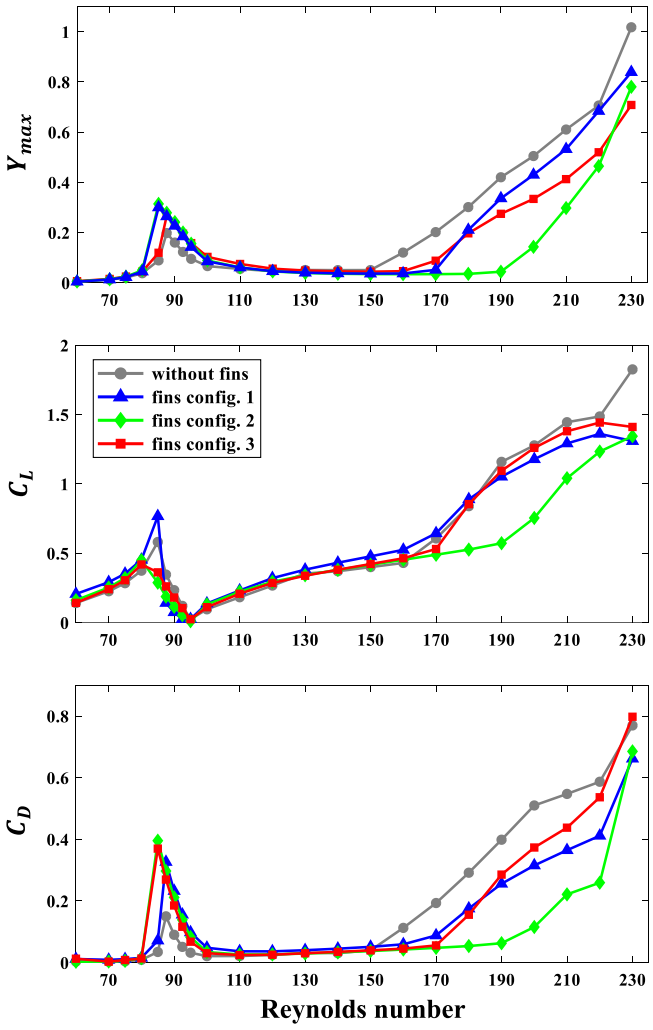

Fig. 4. The variations in the maximum displacement, lift and drag coefficients as a function of Reynolds number for the small fins of Configs. 1–3.

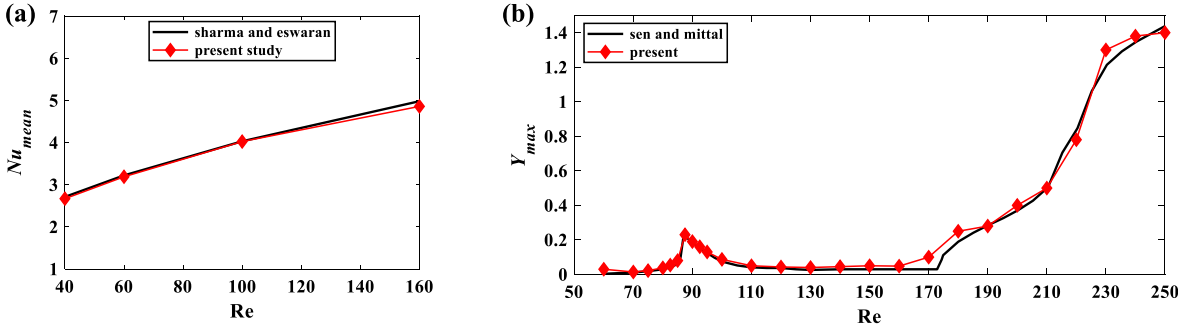

Fig. 3. a) Mean Nusselt number in terms of Reynolds number, and b) Maximum transverse displacement of the square cylinder in terms of Reynolds number.

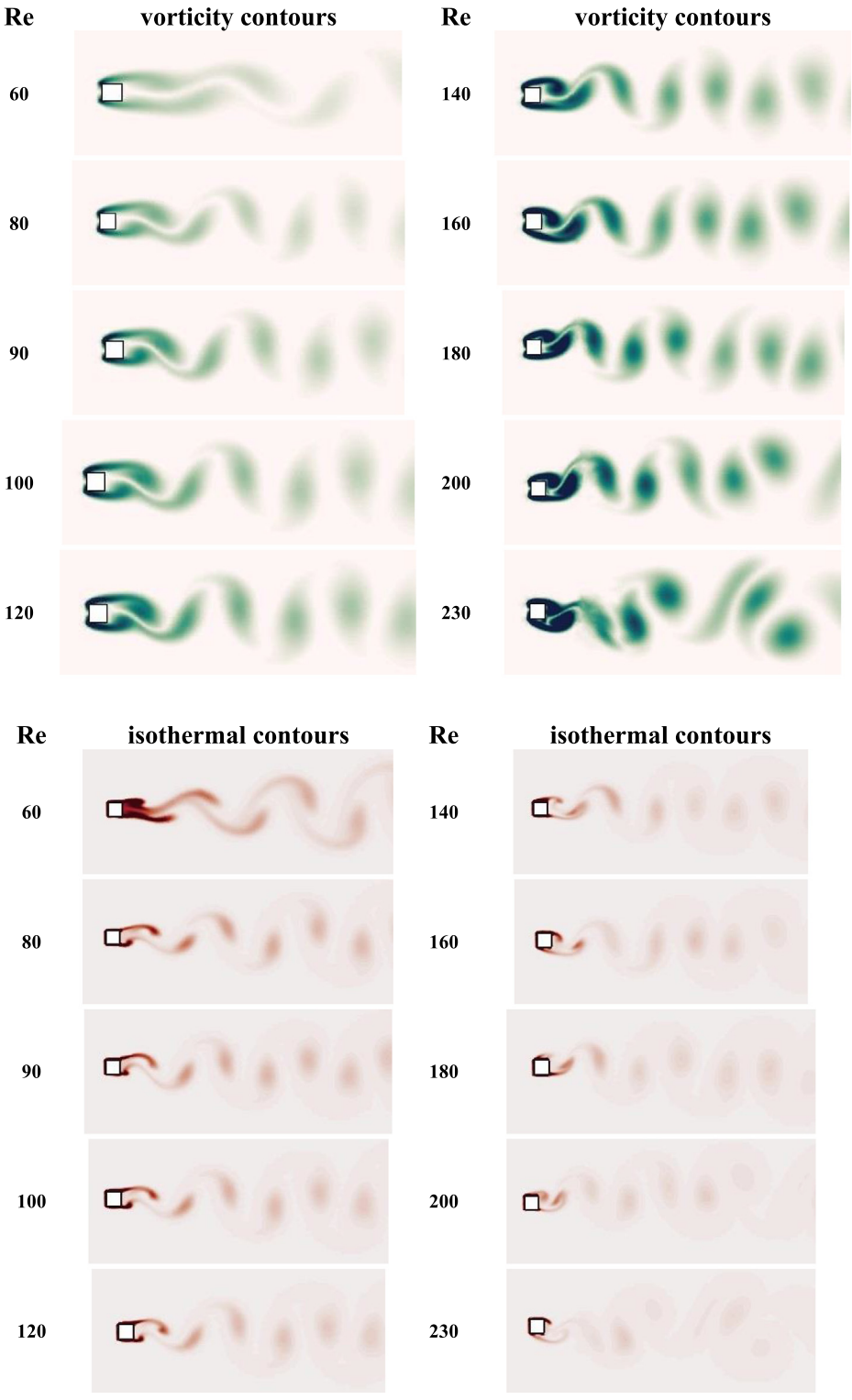

Fig. 5. The vorticity and isothermal contours in the fully developed state as a function of Reynolds number for the non-finned cylinder.

For the square cylinder equipped with small fins in Config. 1, which employs four fins in the cylinder corners, the maximum VIV amplitude increases by 36 % compared to that of plain cylinder. Then, the flow velocity increases and after the cylinder exits the lock-in region, it enters the galloping zone at Re = 160. One observes that the amplitude of cylinder oscillations in the galloping zone decreases by 39 % on average.

For the square cylinder equipped with small fins in Config. 2 where the fins are moved a little backward from the cylinder corners, the lock-in region widens slightly and starts at lower flow velocities than those of plain cylinder. Also, the maximum VIV amplitude increases by 57 %. Thereafter, the galloping zone initiates at higher flow velocities than those of plain cylinder (from Re = 190). Here, the cylinder oscillation amplitude in the galloping

zone decreases by 64 % on average. Finally, the square cylinder equipped with small fins in Config. 3, where the fins are placed next to each other in double arrangement in the middle of top and bottom sides of the cylinder, is investigated. Here, similar to the previous configurations, the maximum VIV amplitude increases by 52 % in comparison with non-finned case. Furthermore, the synchronization region expands which was also observed in Config. 2. Nevertheless, the vibration behavior of this cylinder in the galloping zone is almost identical to that of the cylinder in Config. 1. Last but not least, the amplitude of cylinder vibrations in the galloping zone which starts at Re = 170 decreases by 30 % on average.

In what follows, the effects of small fins in different configurations on force coefficients are evaluated. The trend of changes in the maximum amplitude of lift coefficient on square cylinder, as expected, is completely in line with the vibration behavior of cylinder. Nonetheless, with increasing flow velocity and after the lock-in region, the amplitude of lift coefficient acquires an increasing trend which is even intensified after the galloping zone. Regarding the small fins in Config. 2 which result in the largest reduction in the galloping amplitude, unlike other configurations, the decrease in the lift coefficient compared with that of the plain cylinder is obvious. Here, the amplitude of the lift coefficient on the cylinder decreases by 31 % on average.

The next observation is that the changes in the drag coefficient for the square cylinder equipped with small fins in all configuration are higher than those of the lift coefficient. Addition of small fins to the cylinder, particularly in Configs. 2 and 3, increases the maximum amplitude of drag coefficient in the lock-in region to a large degree in comparison with the plain cylinder. This is followed by a behavior similar to what was observed in the cylinder oscillations amplitude; both in terms of the Reynolds number at which the galloping zone starts, and in terms of the average value of galloping amplitude over the entire studied area.

Fig. 5 shows the vorticity and isothermal contours in the fully developed state at different Reynolds numbers for the plain cylinder (without fins). For lower Reynolds numbers ($60 < Re < 80$), one observes that the vortices are alternately shed from the top and bottom corners of the cylinder, indicating the 2S mode of vortical structure. As the Reynolds number increases, the distance between the vortices gradually decreases and the size and strength of vortices increase. As long as the cylinder is outside of the galloping zone, the vortex-shedding mode remains 2S. After the cylinder enters the galloping zone, it can be seen that the vortex-shedding mode gradually changes from 2S to 2P + 2S. In the 2P + 2S vortex-shedding mode, two vortices from one surface and one vortex from another surface, are alternately shed during a complete vibration cycle, which is especially recognizable for $Re > 190$.

Moreover, according to the isothermal contours, the change in these contours is similar to that in vorticity contours. With increasing Reynolds number, the size and intensity of vortices grow. The vortices detach from the sides of the cylinder which include the hot fluid. In addition, the rise in the size and intensity of vortices mixes up the fluid and increases the average fluid temperature. The start of galloping zone and the change in the vortex-shedding mode intensifies this effect.

Fig. 6 displays the variations in the amplitude of Nusselt number $\widetilde{Nu} = (Nu_{max} - Nu_{min})/2$ and the mean Nusselt number Nu_{mean} as a function of Reynolds number for a cylinder with small fins in Configs. 1–3. For the sake of compromise, the thermal response of the plain cylinder is also involved. It can be seen that in the synchronization and galloping regions, the amplitude of the Nusselt number fluctuations of the finned cylinder is greater than that of the non-finned case. With increasing Reynolds number, the average Nusselt number grows as a higher Reynolds number yields a stronger and more intense turbulence in the cylinder wake. This is also accompanied by a greater average fluid temperature. The values of the mean Nusselt number of the finned cylinder is greater than that of the cylinder without fin, and the values of this growth for Configs. 1–3 are 85 %, 70 % and 66 %, respectively. The highest increase in the mean Nusselt number of the finned cylinder compared to the non-finned cylinder occurs in the galloping zone. The maximum growth value of the mean Nusselt number in the finned cylinder belongs to Config. 1.

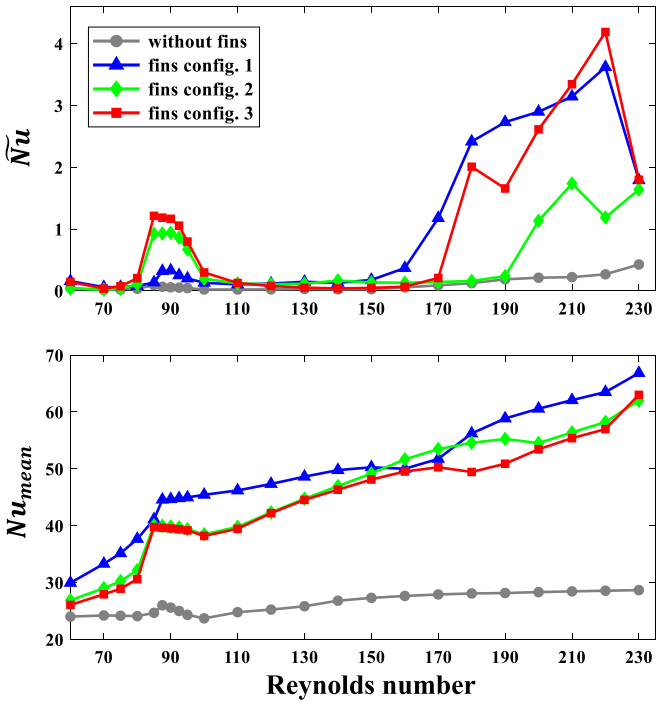

Fig. 6. The variations in the amplitude and mean of Nusselt number as a function of Reynolds number for the small fins of Configs. 1–3.

Fig. 7 shows the effect of adding small fins with different configurations on the vorticity contours of square cylinder at different Reynolds numbers. For a better understanding, the plots of the changes in cylinder displacement (Fig. 4) and the vorticity contours of plain cylinder (Fig. 5) should be considered simultaneously. The trend of the reduction in the distance between vortices in the 2S vortex-shedding mode for cylinders with small fins in Configs. 2 and 3 is observed at lower Reynolds numbers. This is attributed to the earlier onset of the lock-in region in these configurations. Another conclusion is the conversion of 2S mode to 2P + 2S, especially for Config. 2 which starts at higher Reynolds numbers. This is also related to the cylinder displacement diagram.

Fig. 8 shows the effect of adding small fins in different configurations on the isothermal contours of square cylinder at different Reynolds numbers. This is better understood by concurrently considering the plot of the changes in displacement and mean Nusselt number and the isothermal contours of plain cylinder. The change in the vortex-shedding mode and the rise in the number and intensity of vortices behind the cylinder increase the turbulence and the width of the area at the back of the cylinder. As mentioned, the vortices contain hot fluid. A growth in their size and strength causes a greater degree of mixing in the computational field and increases the average fluid temperature. This effect is enhanced by entering the galloping zone and the subsequent change in the vortex-shedding mode.

Fig. 9a displays the variations in the maximum non-dimensional motion of the cylinder with Reynolds number for

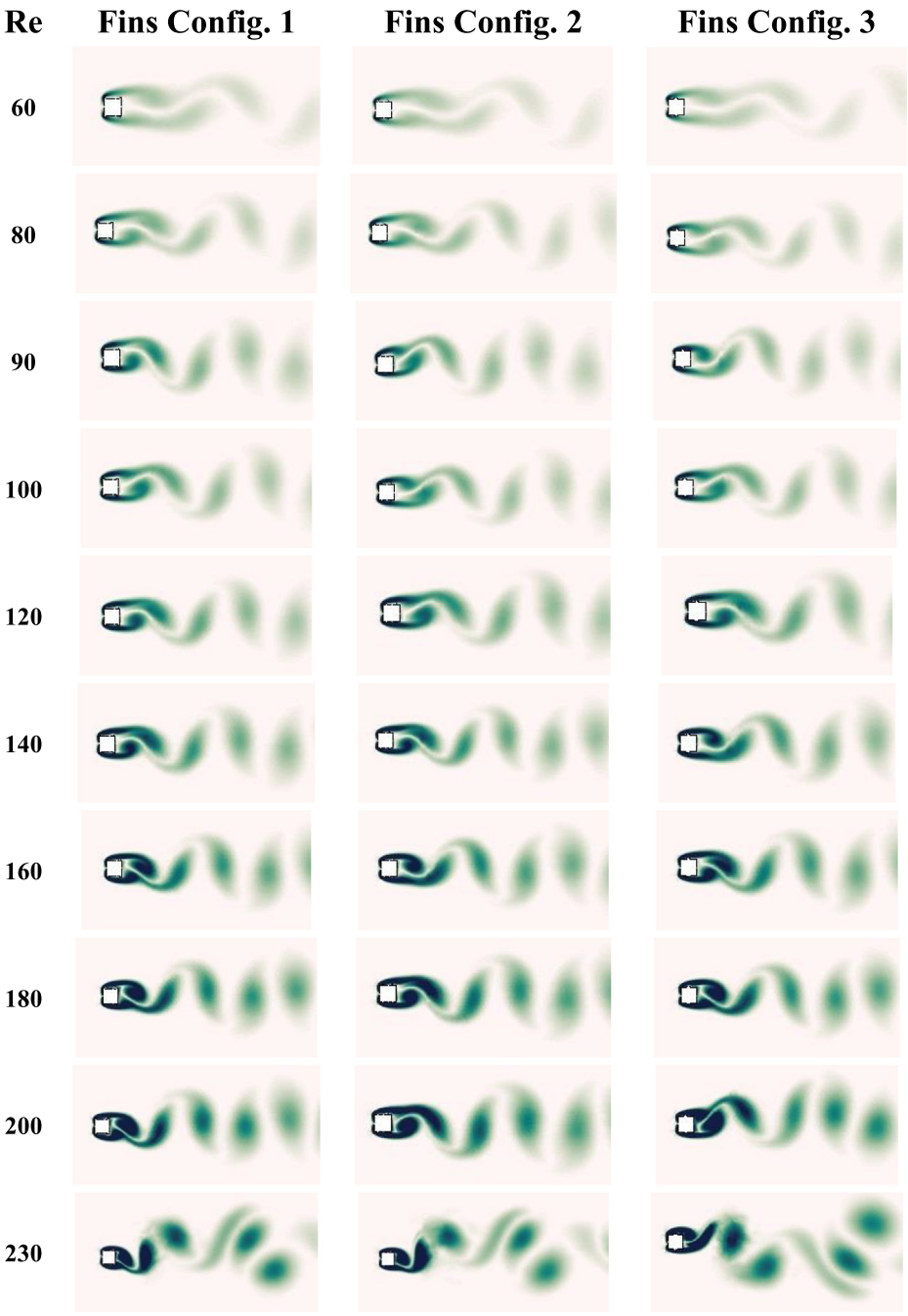

Fig. 7. The vorticity contours in the fully developed state as a function of Reynolds number for the cylinder with small fins of Configs. 1–3.

big fins in Configs. 1–3. Also shown are the changes in the lift and drag coefficients on the cylinder as a function of Reynolds number. For all cases, the response of plain cylinder is added for comparison. As can be seen, adding big fins to the cylinder further increases the VIV amplitude in the lock-in region compared with what is observed for small fins. In addition, the lock-in region expands to a greater degree in comparison to the plain cylinder, particularly in Configs. 2 and 3. In fact, the addition of big fins to the square cylinder makes the maximum oscillation amplitude in the lock-in region approach the values associated with circular cylinder (Fig. 3a in reference [37]).

By contrast, adding big fins has a profound impact on the reduction of galloping amplitude such that the amplitude of square cylinder in the galloping zone for big fins in Configs. 2 and 3 decreases by 87 % on average compared to the plain cylinder case. The corresponding value for small fins reaches a maximum of 64 % in the best scenario. One observes here that adding big fins produces two conflicting effects on the cylinder's vibration response: increasing the VIV amplitude and perfectly attenuating the galloping amplitude. Given the more critical condition of square cylinder in the galloping zone compared to the lock-in region (i.e. larger amplitude and wider coupling area), it seems that the reduction of galloping amplitude has priority.

In the following, the effect of big fins in different configurations on the lift and drag coefficients is reevaluated. Here, one observes again that the changes in the maximum magnitude of lift coefficient are related to the vibration magnitude of the square cylinder. The increase in the lift coefficient amplitude is evident in the lock-

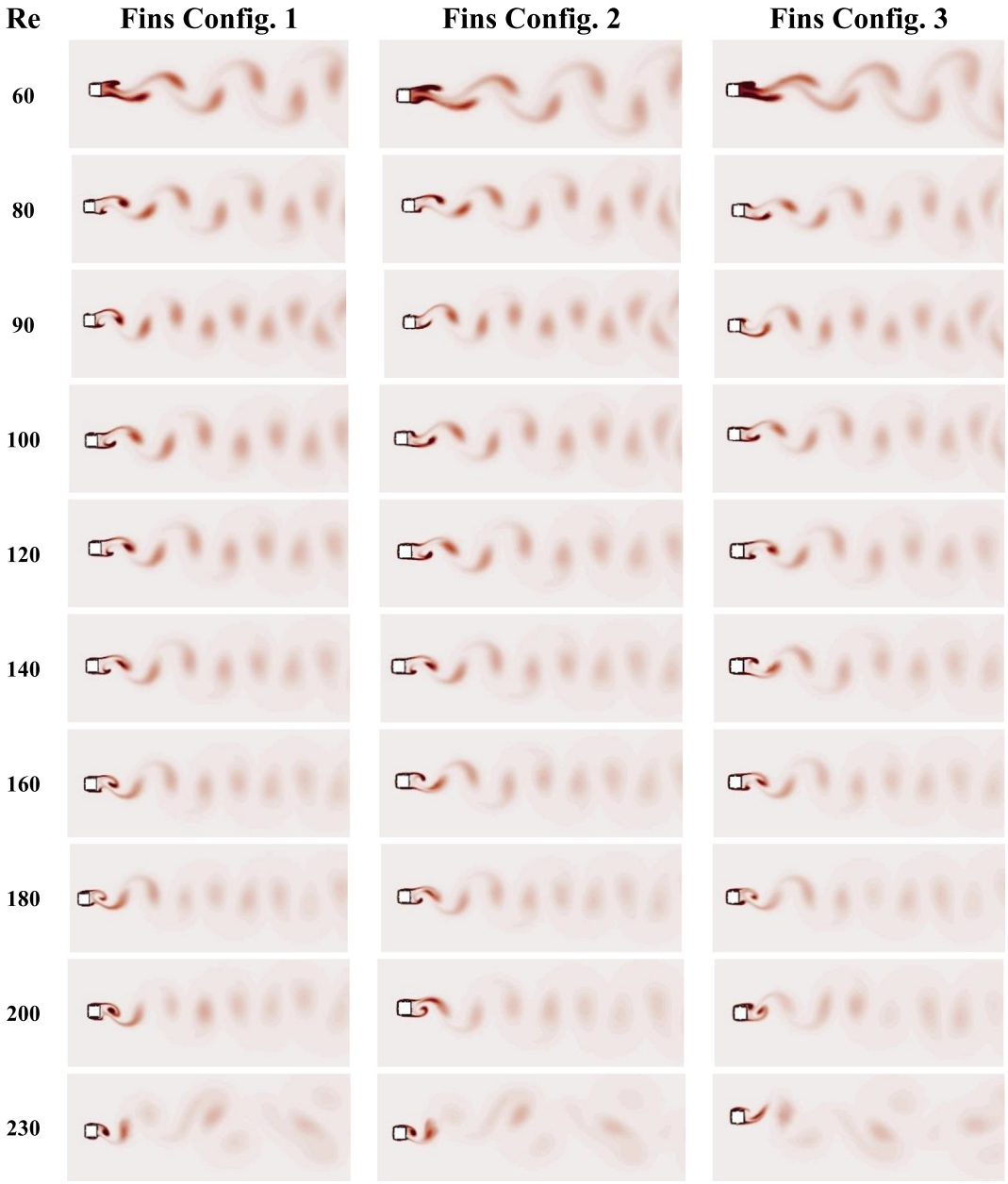

Fig. 8. The isothermal contours in the fully developed state as a function of Reynolds number for the cylinder with small fins of Configs. 1–3.

in region, whereas a decrease in the galloping region is expected. For example, the magnitude of lift coefficient on the cylinder equipped with big fins in Config. 2 is reduced by an average of 43 % in the galloping zone compared to the plain cylinder. Similarly, the drag coefficient changes are greater when the fins, especially big ones, are added. The multiplication of the drag coefficient amplitude in the lock-in region and its significant decrease in the galloping zone are clear.

Fig. 9b displays the variations in the amplitude of Nusselt number $\tilde{Nu} = (Nu_{max} - Nu_{min})/2$ and the mean Nusselt number Nu_{mean} with Reynolds number for a cylinder with big fins in Configs. 1–3. For the sake of compromise, the thermal response of the plain cylinder is also involved. With increasing fin size, the amplitude of Nusselt number in the lock-in region sees a notable jump, while it decreases at higher Reynolds numbers with the reduction in the galloping amplitude in comparison with the case of a cylinder with smaller fins. The maximum value of amplitude changes in two cases of Big fins Config. 2 and Config. 3 occurs at a smaller Reynolds number compared to the case of Big fins Config. 1. In this scenario, unlike the cylinder with small fins, the largest growth in the mean Nusselt number belongs to the case of Config. 3. In the galloping zone, the mean Nusselt number for the cylinder with big fins is lower than the cylinder with small fins. The reason behind this thermal behavior is that the changes in the Nusselt number are straightly proportional to the magnitude of cylinder displacement. Furthermore, the amplitude of oscillations for the cylinder with big fins is lower than that of the cylinder with small fins.

4. Conclusion

The current article focuses on the numerical investigation of the free vibration and heat transfer of a finned square cylinder. These fins have the same shape as shark fins and are located on the top and bottom surfaces of the cylinder. The effects of the size and position of fins on the vortex-shedding, heat transfer and FIV of

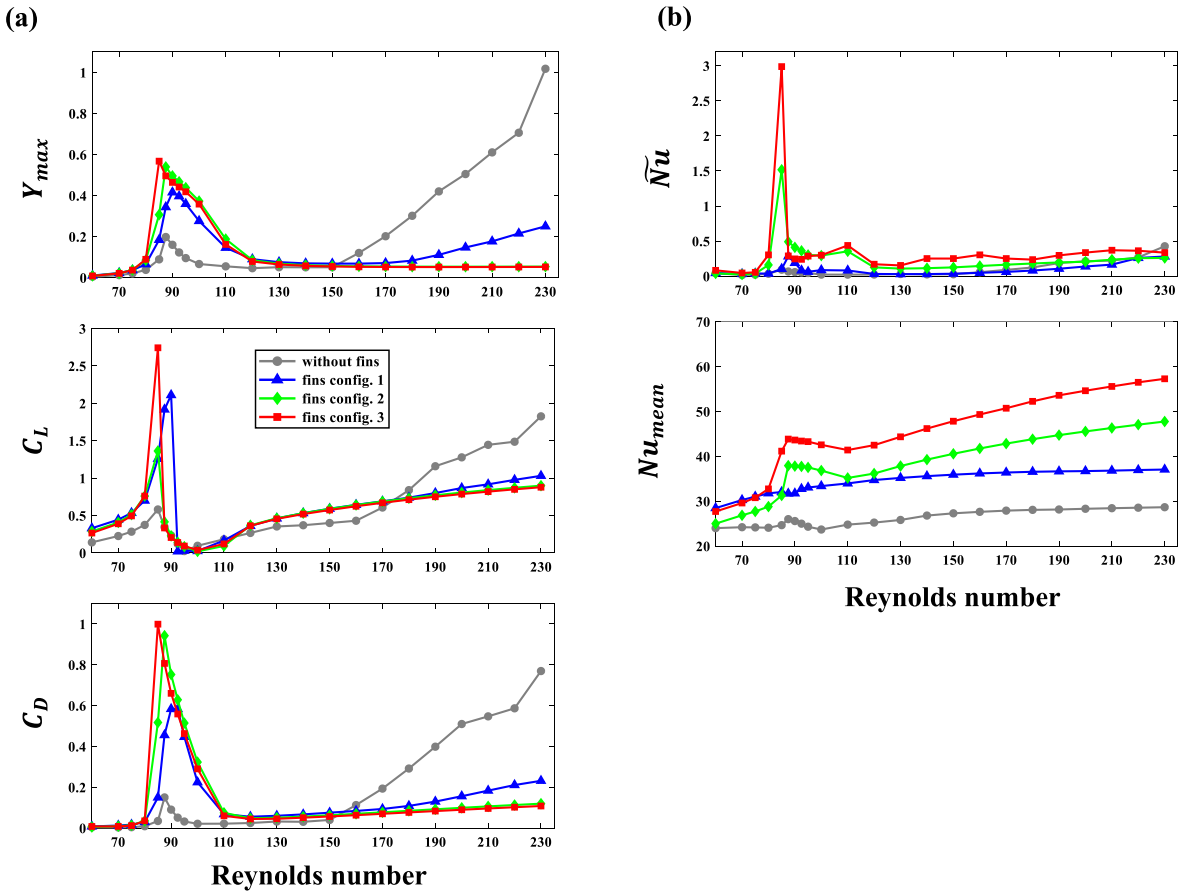

Fig. 9. The changes in the maximum displacement, lift and drag coefficients, the amplitude and mean of Nusselt number as a function of Reynolds number for the big fins of Configs. 1–3.

cylinder in both synchronization and galloping regions are studied. The main results are summarized as follows:

4.1. Effect of small fins on vibration response and vortical structure

For the square cylinder equipped with small fins in Configs. 1–3, the maximum VIV amplitude increases by, respectively, 36 %, 57 % and 52 % compared with the plain cylinder. Furthermore, the galloping zone starts at higher velocities, particularly in Config. 2. Furthermore, the magnitude of galloping oscillations for the cylinder with small fins in Configs. 1–3 decreases by 39 %, 64 % and 30 %, respectively. Also, the trend of reduction in the distance between vortices in the 2S vortex-shedding mode for cylinders with small fins in Configs. 2 and 3 is observed at lower Reynolds numbers as the lock-in region starts earlier in these configurations. Also, the 2S mode transforms into 2P + 2S, which specifically starts at higher Reynolds number for Config. 2 and is related to the plot of changes in the cylinder displacement.

4.2. Effect of big fins on the vibration response and vortical structure

Adding big fins to the cylinder further increases the VIV amplitude in the lock-in region compared to what is seen for small fins. The synchronization region is also much wider than that of plain cylinder, especially in Configs. 2 and 3. On the other hand, the addition of big fins has a great impact on reducing the galloping amplitude so that on average, the square cylinder amplitude in the galloping zone for big fins in Configs. 2 and 3 decreases by 87 % in comparison with the plain cylinder. By contrast, the same quantity in the best case for small fins reaches 31 %.

Also, the trend of reduction in the distance between vortices in the 2S vortex-shedding mode for cylinders with small fins in Configs. 2 and 3 is observed at lower Reynolds numbers. Also noteworthy is the proximity of the 2S vortex-shedding mode to C(2S) for a cylinder in Config. 2 at Re = 87.5, which is the same as the vortex-shedding mode of a circular cylinder at the peak of the lock-in region. This temporary mode change is due to the significant rise in the VIV amplitude of square cylinder equipped with big fins in Config. 2 at this Reynolds number. Another point of interest is that the vortex shedding mode remains 2S for big fins in Configs. 2 and 3 and the conversion to the 2P + 2S mode does not occur. This is explained by the significant reduction of galloping amplitude, although the 2P + 2S mode is of course seen in Config. 1 at higher Reynolds numbers.

4.3. Effect of small and big fins on heat transfer

Adding fins to the square cylinder clearly increases the amount of heat transfer compared with the no-fin case. A higher Reynolds number results in a greater mean Nusselt number. The highest increase in the mean Nusselt number of the finned square cylinder occurs in the galloping zone. The fin size affects the vortical structure mode and the amplitude of cylinder displacement. The use of big fins causes the greatest changes in the Nusselt number amplitude for Configs. 2 and 3 take place in the lock-in region and at Re = 87.5. Regarding small and big fins, the highest growth in the mean Nusselt number belongs to, respectively, Configs. 1 and 3. Finally, in the galloping zone, the mean Nusselt number of the cylinder with small fins is higher than that of the cylinder with big fins.

Declaration of Competing Interest

The authors declare that they have no known competing financial interests or personal relationships that could have appeared to influence the work reported in this paper.

References

[1] Sarpkaya T. A critical review of the intrinsic nature of vortex-induced vibrations. J Fluids Struct 2004;19(4):389–447.
[2] Rabiee AH, Farahani S. A comprehensive study of heat transfer characteristic and two-dimensional FIV for heated square-section cylinder with different damping ratios. Int Commun Heat Mass Transfer 2020;116:104680.
[3] Carberry J, Govardhan R, Sheridan J, Rockwell D, Williamson CH. Wake states and response branches of forced and freely oscillating cylinders. Eur J Mech-B/Fluids 2004;23(1):89–97.
[4] Rabiee AH, Esmaeili M. Simultaneous vortex-and wake-induced vibration suppression of tandem-arranged circular cylinders using active feedback control system. J Sound Vib 2020;469:115131.
[5] Garg H, Soti AK, Bhardwaj R. Thermal buoyancy induced suppression of wake-induced vibration. Int Commun Heat Mass Transfer 2020;118:104790.
[6] Rabiee AH, Farahani SD. Effect of synthetic jet on VIV and heat transfer behavior of heated sprung circular cylinder embedded in a channel. Int Commun Heat Mass Transfer 2020;119:104977.
[7] Al Omari S, Ghazal A, Elnajjar E, Qureshi Z. Vibration-enhanced direct contact heat exchange using gallium as a solid phase change material. Int Commun Heat Mass Transfer 2020:104990.
[8] He W, Nie S, Meng T, Liu Y-J. Modeling and vibration control for a moving beam with application in a drilling riser. IEEE Trans Control Syst Technol 2016;25(3):1036–43.
[9] Gao Y, Yang J, Xiong Y, Wang M, Peng G. Experimental investigation of the effects of the coverage of helical strakes on the vortex-induced vibration response of a flexible riser. Appl Ocean Res 2016;59:53–64.
[10] Hasheminejad SM, Rabiee AH, Bahrami H. Active closed-loop vortex-induced vibration control of an elastically mounted circular cylinder at low Reynolds number using feedback rotary oscillations. Acta Mechanica 2018;229(1):231–50.
[11] Hasheminejad SM, Rabiee AH, Markazi A. Dual-Functional Electromagnetic Energy Harvesting and Vortex-Induced Vibration Control of an Elastically Mounted Circular Cylinder. J Eng Mech 2017;144(3):04017184.
[12] Chen Y, Song Z, Li F. Generating mechanism of mode localization for the beams and its application in the passive vibration control. J Sound Vib 2020;485:115531.
[13] Assi GR, Bearman PW. Vortex-induced vibration of a wavy elliptic cylinder. J Fluids Struct 2018;80:1–21.
[14] Owen JC, Bearman PW, Szewczyk AA. Passive control of VIV with drag reduction. J Fluids Struct 2001;15(3–4):597–605.
[15] Constantinides Y, Oakley OH Jr. Numerical prediction of bare and straked cylinder VIV. In: International Conference on Offshore Mechanics and Arctic Engineering, 2006, pp. 745-753.
[16] Zeinoddini M, Farhangmehr A, Seif M, Zandi A. Cross-flow vortex induced vibrations of inclined helically straked circular cylinders: An experimental study. J Fluids Struct 2015;59:178–201.
[17] Huera-Huarte F. Suppression of vortex-induced vibration in low mass-damping circular cylinders using wire meshes. Mar struct 2017;55:200–13.
[18] Senga H, Larsen CM. Forced motion experiments using cylinders with helical strakes. J Fluids Struct 2017;68:279–94.
[19] Aguirre-López MA, Hueyotl-Zahuantitla F, Morales-Castillo J, Santos GJE, Almaguer F-J. Simulating the flow around a baseball: Study of a 2D-cylinder with a single bump. Comput Math Appl 2019;78(9):3105–16.
[20] Xu W-H, Yang M, Ai H-N, He M, Li M-H. Application of Helical Strakes for Suppressing the Flow-Induced Vibration of Two Side-by-Side Long Flexible Cylinders. China Ocean Eng 2020;34:172–84.
[21] Kang S, Ryu S, Song S. Quantification of VIV-driven energy transfer for a circular cylinder with a pair of bumps at Reynolds number 150. J Mech Sci Technol 2020:1–9.
[22] Rabiee AH. Galloping and VIV control of square-section cylinder utilizing direct opposing smart control force. J Theor Appl Vibration Acoust 2019;5(1):69–84.
[23] Wu C-H, Ma S, Kang C-W, Lim T-B-A, Jaiman RK, Weymouth G, et al. Suppression of vortex-induced vibration of a square cylinder via continuous twisting at moderate Reynolds numbers. J Wind Eng Ind Aerodyn 2018;177:136–54.
[24] Dash SM, Triantafyllou MS, Alvarado PVY. A numerical study on the enhanced drag reduction and wake regime control of a square cylinder using dual splitter plates. Comput Fluids 2020;199:104421.
[25] Song Hu Q, Xi Zhou S, Yu Zhang S. Biomimetic Robotic Fish Fins Propulsion Modes Research in Flow Field. In: 2013 International Conference on Advanced Computer Science and Electronics Information (ICACSEI 2013). Atlantis Press; 2013.
[26] Liu G, Geng B, Zheng X, Xue Q, Dong H, Lauder GV. An image-guided computational approach to inversely determine in vivo material properties and model flow-structure interactions of fish fins. J Comput Phys 2019;392:578–93.
[27] Ding L, Yang L, Yang Z, Zhang L, Wu C, Yan B. Performance improvement of aeroelastic energy harvesters with two symmetrical fin-shaped rods. J Wind Eng Ind Aerodyn 2020;196:104051.
[28] Macias MM, Souza IF, Junior ACB, Oliveira TF. Three-dimensional viscous wake flow in fish swimming-A CFD study. Mech Res Commun 2020;103547.
[29] Zhu H, Gao Y. Hydrokinetic energy harvesting from flow-induced vibration of a circular cylinder with two symmetrical fin-shaped strips. Energy 2018;165:1259–81.
[30] Hatami M, Safari H. Effect of inside heated cylinder on the natural convection heat transfer of nanofluids in a wavy-wall enclosure. Int J Heat Mass Transf 2016;103:1053–7.
[31] Hatami M, Sheikholeslami M, Domairry G. High accuracy analysis for motion of a spherical particle in plane Couette fluid flow by multi-step differential transformation method. Powder Technol 2014;260:59–67.
[32] Mehryan S, Izadpanahi E, Ghalambaz M, Chamkha A. Mixed convection flow caused by an oscillating cylinder in a square cavity filled with Cu–Al2O3/water hybrid nanofluid. J Therm Anal Calorim 2019;137(3):965–82.
[33] Mehryan S, Goudarzi P, Zadeh SMH, Ghodrat M, Younis O, Ghalambaz M. Thermal vibrational and gravitational analysis of a hybrid aqueous suspension comprising Ag–MgO hybrid nano-additives. Int Commun Heat Mass Transfer 2021;126:105345.
[34] Ghalambaz M, Mehryan S, Izadpanahi E, Chamkha AJ, Wen D. MHD natural convection of Cu–Al2O3 water hybrid nanofluids in a cavity equally divided into two parts by a vertical flexible partition membrane. J Therm Anal Calorim 2019;138(2):1723–43.
[35] Prasanth T, Mittal S. Vortex-induced vibrations of a circular cylinder at low Reynolds numbers. J Fluid Mech 2008;594:463–91.
[36] Sen S, Mittal S. Free vibration of a square cylinder at low Reynolds numbers. J Fluids Struct 2011;27(5–6):875–84.
[37] Hasheminejad SM, Rabiee AH, Jarrahi M, Markazi A. Active vortex-induced vibration control of a circular cylinder at low Reynolds numbers using an adaptive fuzzy sliding mode controller. J Fluids Struct 2014;50:49–65.
[38] Sharma A, Eswaran V. Heat and fluid flow across a square cylinder in the two-dimensional laminar flow regime. Numer Heat Trans, Part A: Appl 2004;45(3):247–69.
[39] Sen S, Mittal S. Effect of mass ratio on free vibrations of a square cylinder at low Reynolds numbers. J Fluids Struct 2015;54:661–78.

Amir H. Rabiee received the M.S. and Ph.D. degrees in mechanical engineering from Iran University of Science and Technology in 2011 and 2017. His research interests focus on active andsemi-active vibration control, data science and intelligent control systems.

S.D. Farahani received the M.S. and Ph.D. degrees in mechanical engineering from Tehran university. His research interests focus on Nanoscale heat transfer, Thermal system modeling, Inverse heat transfer problem, Optimization, Two-phase flow, Heat transfer modeling in Machining Process.

Dr. Mosavi is a data scientist at Obuda University where he forms a research group with the collaboration of IEEE members.